

Heartbeat Aware Decoding in Molecular Networks

Jiaming Wang^{*}, Samin Beheshti Zavareh[†], Haitham Hassanieh[‡] and Bhuvana Krishnaswamy[§]

^{*} University of Illinois at Urbana-Champaign, Email: jw27@illinois.edu

[†] University of Bern, Email: samin.beheshti@students.unibe.ch

[‡] École Polytechnique Fédérale de Lausanne, Email: haitham.alhassanieh@epfl.ch

[§] University of Wisconsin-Madison, Email: bhuvana@ece.wisc.edu

Abstract—Molecular communication (MC) is a competitive candidate of implementing the long-lasting in-body communication for the body-area medical network, considering its unparalleled advantages over conventional wireless communication in bio-compatibility. Blood vessel is a common topic and the influence of blood flow on the propagation of molecular signals has been studied. However, one of the most significant features was overlooked by all past work—blood is a periodic flow with varying rate, so the channel response varies across time. This is similar to the fast-varying channel in conventional wireless systems, but the molecular condition could be much worse because the channel can vary from symbol to next, so using average flow speed for approximation is far from reality. This paper proposes FlowLink to compensate for the drastic channel variation. FlowLink employs a flow meter and records the real-time flow rate, which accumulates over time and forms a “flow axis”. By resampling the receiver signal on this flow axis with a fixed flow interval, FlowLink compensates for the varying channel response and restores the coherence time requirement for packet-based communication. FlowLink is evaluated on a vessel-like testbed with a periodic flow mimicking blood, which demonstrates an average improvement in decoding BER of 40% compared to conventional flow-unaware decoder.

Index Terms—communication, wireless communication, molecular communication, decoding, heartbeat, blood flow.

I. INTRODUCTION

Molecular networks are a new paradigm for communication using molecules inside the human body [1]–[6]. They are set to play a crucial role in advancing healthcare by allowing us to communicate with biological micro- and nano-implants [7]–[9]. These implants include biosensors for continuous monitoring [10]–[12], nano-scale Lab-on-a-Chip for in body medical diagnosis [13]–[15], biological nano-machines that can detect microbes [16]–[18], and nano-robots that can travel in blood vessels to perform targeted drug delivery [13], [19], [20].

The idea behind molecular networks is very simple: implants can communicate by releasing molecular particles into the bloodstream. For example, we can encode a “1” bit by releasing particles and a “0” bit by releasing nothing. Molecular networks form a more suitable alternative to wireless networks, traditionally used for communication with larger medical implants such as pacemakers and indigestible pill cams [21], [22]. Conventional wireless solutions are not the ready-to-use technique, because the radios are too large and consume too much power for micro- and nano-implants [23]–[25]. Molecular devices, on the other hand, have a small form factor and are bio-compatible as they are built using synthetic

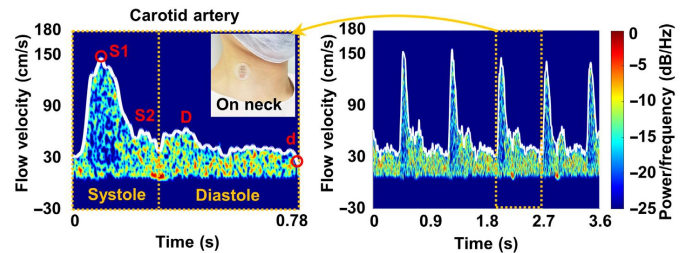


Fig. 1: Ultrasonic spectrum for carotid artery [39].

cells, genetically engineered bacteria, or biological circuits that can send and receive particles [26]–[33].

The massive progress in bio-research that made such implants and molecular bio-transceivers practical has recently generated interest from communication and networking systems researchers in designing and testing protocols for molecular networks in synthetic experimental testbeds that emulate vessels and blood flow [34]–[38]. Although these works have made concrete contributions to the development of molecular networks in the blood stream, one major feature of the channel has been ignored—the blood flow speed is not a constant. Previous work has observed and addressed the potential gradual channel variation during packet transmission [35], but did not account for the rapid channel variation due to heartbeats which can degrade the performance of conventional decoders.

The heart iterates between two stages—diastole, when the chambers relax and refill with blood, and systole, when the chambers contract and push blood into the artery. Figure 1 shows the medical ultrasonic spectrum image that measures the blood speed variation. It can be seen that systole is accompanied by a sudden increase in the blood flow speed, which will gradually reduce during diastole stage. Considering that (1) the normal heart rate of an adult is between 60 and 100 beats per minute (≈ 1 to 1.6 beats per second) and (2) data rates of a few bits per second have been demonstrated in a vessel like system [35], [40], the blood flow cycle is roughly as long as the MC symbol interval if not longer. Hence, the MC channel could change within symbols and the assumption in conventional wireless systems, that the channel does not change during the transmission of one packet, no longer holds. Even though fast-varying channels have been studied in electromagnetic and acoustic communication systems, the propagation speed of the signal is typically constant and the variation is usually limited to phase change of Channel Impulse Response (CIR) taps which can be tracked with pilots.

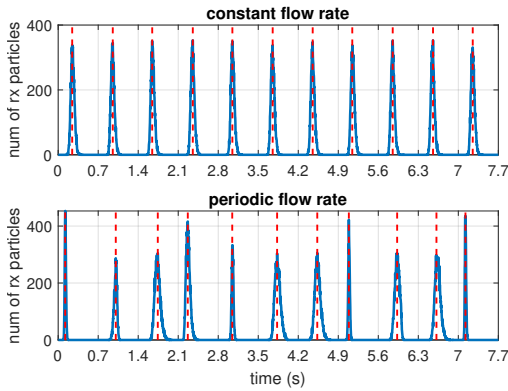


Fig. 2: The number of particles detected at the receiver end under constant flow (above) and heartbeat-induced flow (below). In both cases, the transmitter sends a train of pulses with a constant interval of 0.7 seconds. It can be seen that under constant flow, the received signal reveals a consistent pattern with a period of 0.7 seconds, which is identical to the transmission rate. However, under the heartbeat-induced flow with a period of 1 second, the signal of each pulse no longer maintains a constant spacing. Moreover, the response of each transmitted pulse also diverges from each other.

MC networks, however, are faced with a more challenging varying channel where the propagation speed of the signal changes between symbols. This causes the boundaries of symbol periods to differ among consecutive symbols. Figure 2 shows an example of the number of received particles when the speed of flow is constant and when it changes due to the heartbeats. As can be seen in the top figure, when the speed is constant, the particles arrive at equal intervals and channel impulse response is uniform. However, with heartbeat, the propagation time of particles can change from symbol to next and the channel impulse response changes. Hence, the boundaries where each symbol starts and ends change depending on the speed of the flow making it difficult to correctly decode the signal. The example shown in Figure 2 is simulated for a relatively low data rate of 1.4 bps i.e. symbol interval of 0.7s and small inter-symbol-interference (ISI) in order to demonstrate how the symbol boundaries shift. In practice, as we increase the data rate and with realistic ISI, it becomes increasingly harder to determine the symbol boundaries as particles from different symbols stack up.

In this paper, we propose FlowLink, a heartbeat-aware MC protocol that compensates for the influence of heartbeats to correctly decode molecular signals. The core idea of FlowLink is to preprocess the received signal to extend the period during high flow speed and shrink it during low flow speed, such that all symbols can be equally sensed by the receiver and share the same CIR. It does so by projecting the received signal on the flow volume axis (i.e. integral of flow speed) which rescales the signal and unifies the CIR of each symbol as we prove in Section IV-A. While this rescaling allows all symbols to experience the same CIR in the flow volume axis, the symbols continue to be non-uniformly separated. The spacing between symbols is determined by the varying flow speed, not only when the receiver senses the symbol, but also when the transmitter sends the symbol. So, the dynamic symbol

boundaries remain on the flow volume scale and prevent decoding. To address the problem, FlowLink begins with packet detection, including a coarse stage using energy detection and a finer stage using signal reconstruction. FlowLink scans over the potential time of transmission reported by the coarse stage—for each sample it infers the corresponding symbol boundaries with real-time flow rate, estimates the CIR with known preamble symbols, reconstructs the signal through convolution and computes its divergence from the received signal—until it finds the minimum error between two signals.

We built a testbed to evaluate the performance of FlowLink, which is modified from the artifact of [41] using a peristaltic pump with MODBUS speed control that allows us to emulate the heartbeats. The dataset contains various scenarios with varying TX-RX distance, flow cycle and channel diameter. By comparing FlowLink with the decoder [41] under the scenario of one TX and one RX, we show that FlowLink can distinguish the accurate symbol period and reduce the decoding BER by an average of 40%.

The paper makes the following contributions. To the best of our knowledge, this is the first MC decoder that accounts for the heartbeats and flow speed variation and does not require any modeling of a channel with specific parameters. We also set up a testbed with varying flow speed to evaluate the performance of FlowLink, which is compared with a conventional decoder under different flow conditions.

II. BACKGROUND

In this section, we will provide some background knowledge on molecular communication. In addition, since different assumptions about the system will lead to different solutions, we will also describe the network model we use here.

A. Propagation of Molecular Signal

The essence of the propagation of molecular signal is the movement of information particles, which has two components—advection and diffusion. Advection refers to bulk motion of an entire body as a consequence of pressure gradient, such as blood flow (liquid) and wind (gas), which can be described by a vector field \vec{v} [m/s]. Diffusion is the movement from a high-concentration region to a low-concentration region, which has no net movement and can be described by the diffusion coefficient D [m²/s]. A typical diffusion coefficient for a molecule in the gas phase is in the range of $10^{-6} - 10^{-5} m^2/s$, while in an aqueous solution $10^{-10} - 10^{-9} m^2/s$. From a macro view, the advection-diffusion equation describes the concentration of information particle c with relation to particle sink/source R .

$$\frac{\partial c}{\partial t} = \nabla \cdot (D \nabla c - \vec{v} c) + R \quad (1)$$

Solving the above equation gives a macro-view description of the movement of a large amount of particles, while another widely adopted Monte-Carlo method is used to simulate the movement of each single particle. With time step Δt , the variation of a particle coordinate follows a normal distribution

$$\Delta x \sim \mathcal{N}(v_x \Delta t, 2\sqrt{D \Delta t}) \quad (2)$$

B. Molecular Network Model

In this paper, we adopt the model that the molecular network in the blood is composed of gateways and nodes. The whole body is divided into multiple areas, and each is serviced by a sub molecular network and managed by a node. The network is the backbone connecting these separate areas, which also bridges the inside network with the outside through the gateways. The nodes and the gateways are immobile. Although uni-directional communication is the common case between one node and one gateway due to the blood flow, bi-directional communication for each node can be implemented by sending to the downstream gateway and receiving from the upstream. We assume the transmitter adopts On-Off Keying (OOK) and releases a pulse ($\delta(t)$) of particles as bit “1”.

The propagation of information particles is advection-dominant, while molecular diffusion has negligible influence. However, this does not mean the Channel Impulse Response (CIR) is a single tap due to the following two major factors. On the one hand, the blood vessel topology is complicated with diameter variation and forking. On the other hand, the blood flow in the vessels is assumed laminar, where the flow speed is higher as is further away from the wall of the vessel. Besides, the information particles do not transform in the channel, and are not destroyed by the receiver. Note that these assumptions best suit the testbed in the work, while more discussions are provided in Section VIII-B.

III. OVERVIEW AND CHALLENGES

Fast time-varying channel is a well-studied topic in conventional wireless communication systems [42] because of the growing user scenarios, especially with the increased user mobility, data rates and carrier frequencies. The movement of transmitter, receiver and reflectors features a significant Doppler effect, and there exist various models and solutions [42]. However, considering the transmission rate of multiple Mbps (i.e. short symbol interval), the object movement is mostly shown in the phase variation of each CIR tap, instead of change in tap delay [43]. This is usually true during the transmission of a standard-size packet.

However, for molecular signals, the propagation delay is multiple-order-of-magnitude longer than conventional wireless signals even with the aid of the environmental flow. Such difference determines that the molecular signal propagation delay in the blood is much longer. Since diffusion of molecular signals will induce large Inter-Symbol Interference (ISI), which is proportional to the propagation delay, the data rate is limited and is generally not competitive with the convention wireless techniques. The long symbol interval provides more opportunity to observe the variation in the environmental flow speed between symbols.

To simplify the illustration of this problem, we assume the channel is 1-D and temporarily ignore the influence of diffusion. Moreover, with the general assumption that liquid is incompressible¹, the variation of speed could instantaneously

¹Molecular communication is a wide area which also covers gas as medium, where compressing is much easier and may not be a common assumption.

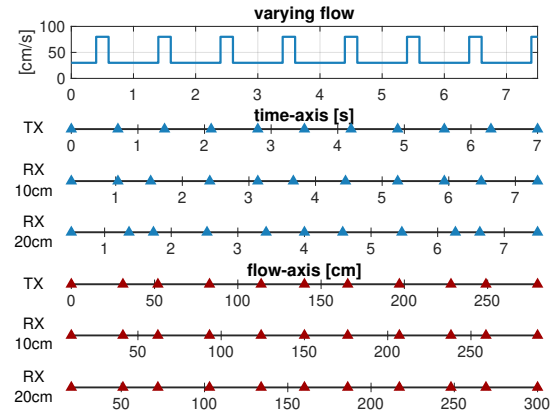


Fig. 3: The arrival time of consecutive symbols of the same MC packet is messed up by the varying flow speed. From top to bottom: (1) the flow speed [cm/s] as a function of time [s]; (2) the pulse train of 0.7s interval sent by TX and received by two RX at 10cm and 20cm, where the blue plots use time-axis and the red plots use flow-axis. To compare the interval between pulses, the axes have the same scale but different ranges.

reflect in every part of the channel. Equation 3 depicts the relation between the transceiver distance Δx and the propagation delay Δt , where $v(t)$ is the flow speed and t_0 is the transmission time of the signal.

$$\Delta x = \int_{t_0}^{t_0+\Delta t} v(t)dt \quad (3)$$

The direct consequence of the varying flow speed is that the symbols in the same packet now bear different propagation delays, so the receiver can no longer use the predetermined symbol interval to mark the start of each symbol. Figure 3 provides a simple example illustrating such influence. The channel is a narrow long tube (1-D), in which runs a periodic flow iterating between 80 cm/s for 0.2 s—mimicking the systole of heart—and 30 cm/s for 0.8 s—mimicking the diastole of heart (Figure 3 top). The TX at $x = 0$ sends a pulse train with an interval of 0.7 s (Figure 3 top second). However, none of the RXs at $x = 10$ cm and $x = 20$ cm (Figure 3 blue plots) receive the same pulse train as transmitted. Moreover, the two RXs do not see the same pattern either, where the complexity lies in the various combinations of different flow profiles as well as the symbol transmission time.

Conventional decoders are not ideal if the arrival time of each symbol is not predictable, especially when the high environmental flow speed could lead to some of the symbols arriving with little interval and compacting within one symbol period. How to compensate for such flow variation is the unique challenge and is not the priority in conventional wireless systems.

IV. TECHNICAL DESIGN

The propagation delay of each symbol is not a constant; in other words, this means that the Channel Impulse Response (CIR) varies across the packet. A simple idea is that decoding is possible if we somehow know the CIR of each symbol. Then the solution is to compute the CIR based on some template

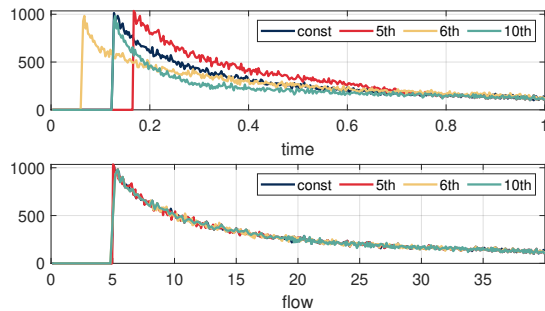


Fig. 4: Monte-Carlo simulated CIR on 1-D channel model. The CIRs for different symbols with time x-axis (upper) are unified by flow amount x-axis (lower), where y-axis is the number of detected particles.

CIR which shrinks during high speed in the time scale and expands during low speed. This is not an incorrect solution, but is followed by a series of complicated and entwined problems: “what is this template CIR?”, “what is the arrival time of each symbol?” and “how can we solve these two problems concurrently when the preamble is not in the regular order?” Instead, we focused on the non-varying factor among the altering CIRs and developed the intuitive decoder FlowLink. In this section, we will explain the two major components of FlowLink which composes the solution to the varying flow.

A. Picking a new x-axis

As was discussed in Section III, in conventional wireless systems, the channel impulse response (CIR) is considered unvarying within the channel coherence time, i.e. the **propagation delay** of each path between transceivers is a constant. Thus, sampling by a fixed **time interval** can maintain the pattern of the original transmitted sequence. From this perspective, what is the constant value in the molecular channel that can inspire the corresponding sampling parameter? The network model described in Section II features a simple answer. Under the assumption of the immobile transceivers and the advection-dominant channel, the **total volume of blood flow** by molecular signals to propagate from the transmitter to the receiver is a constant. Consequently, instead of treating the receiver signal as a function of time $y(t)$, FlowLink first converts it to a function of flow $y(V)$.

To understand the effectiveness of such x-axis replacement, let’s start with an example assuming an advection-only 1-D channel model where the CIR is a single pulse. It is easier to understand in 1-D, because flow rate $Q(t)$ [volume per time (m^3/s)] can be reduced to $v(t)$ [distance per time (m/s)], which is directly related to the molecular propagation model described in Section II. Let’s go back to Figure 3 and focus on the red plots, which are the identical RX signal but using flow amount as the x-axis. It can be seen that the receivers can capture the same pulse train as it was sent by the transmitter on the flow-axis, regardless of the propagation distance.

But, does the flow-axis solve the problem when the CIR is much more complicated like in a real blood channel? Figure 4 provides a simple Monte-Carlo simulation for the receiver at $x = 10$ cm as in Figure 3, but in a 3-D tube-like channel

with laminar flow. Figure 4(upper) first plots the CIR when the flow rate is a constant that is equal to the average speed of the varying flow (in blue), while the other three curves depict the CIR of the 5th, 6th and 10th pulse respectively. As can be seen, the varying flow not only affects the propagation delay and delay of each symbol, but also the width of the CIR, which is usually accompanied by an abrupt shape change between systole and diastole. On the contrary, in Figure 4(lower), the CIR of different pulses perfectly overlaps with each other.

How do we get the receiver signal $y(V)$? From the algorithm’s perspective, the easiest solution is to equip the device with a flow meter module (Section VIII-C provides some possibilities on flow estimation without a flow meter.) It is reasonable to assume that the blood flow is uni-directional in most cases, so $Q(t) > 0$ and $V(t) = \int_0^t Q(t)$ is monotonically increasing and there exists the inverse function $t = f(V)$. Thus, we can directly use the flow meter to preprocess the signal and achieve $y(f(V))$. This is the solution we use to measure the ground truth in the testbed. To compensate for the non-uniform distribution of time samples on the flow-axis, FlowLink first adopts a higher sampling rate than the symbol rate and then computes the uniform flow samples through interpolation.

Here are a few remarks on using the flow-axis. First, it should be noticed that there is no one-to-one mapping between the time samples and the flow samples, because the blood flow is not a variable with discrete values. Thus, FlowLink relies on a simple observation—concluded from past works—that the CIR can be linearly interpolated under a high flow sampling rate, which enables the Viterbi algorithm with a few modifications. It maps one time pulse into no more than two flow pulses. Typically, a time pulse $\delta(t)$ can be approximated by

- If $k = \frac{V(t)}{\Delta V}$ is an integer, where ΔV is the flow sampling interval

$$\delta(t) \mapsto \delta[k] \quad (4)$$

- Otherwise, $k = \lfloor \frac{V(t)}{\Delta V} \rfloor$

$$\delta(t) \mapsto \left(k + 1 - \frac{V(t)}{\Delta V}\right) \delta[k] + \left(\frac{V(t)}{\Delta V} - k\right) \delta[k + 1] \quad (5)$$

Second, although the above illustration assumes that the channel is a single tube of constant diameter, the FlowLink method can generalize to other complicated channel topologies, with either varying cross sections or forking. In spite of the elasticity of the blood vessels, the topology is comparably stable when the person is static. Thus, it is reasonable to assume that the distribution of the blood flow in this network is also stable during the transmission of a packet, such that a large amount of information particles follows the same statistical distribution during propagation, which leads to an unvarying CIR. Besides, it should be noted that the receiver may sense a different amount of blood flow from the transmitter due to the forking in the blood vessels. But, since the stable topology indicates that the blood flow at different devices should maintain a constant ratio, the receiver

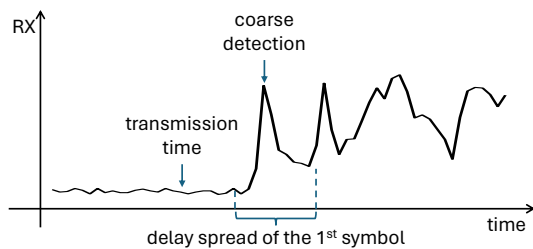


Fig. 5: The relationship between coarse detection, delay spread and transmission time.

only needs to resample the signal based on its own flow measurement $V_R(t)$, without any knowledge about the one at the transmitter end $V_T(t)$. The related benchmarks will be presented in Section VI-B4.

B. Detecting the symbol boundaries

Even though the CIR of each symbol is unified, another problem prevents the usage of conventional decoders. Although the symbols are sent by the transmitter with a fixed time interval, the propagation delay between the transmitter and the receiver for each symbol is a variable, which is decided by the varying flow rate and leads to the uneven spacing between symbols at the receiver end (as depicted in Figure 3). Failing to resolve the floating symbol boundaries can lead to improper handling of inter-symbol interference (ISI), which will further deteriorate the receiver’s performance.

It may seem very complicated at first glance that we need to decide the duration for each symbol, because there are usually hundreds of symbols in one data packet and the wrong detection of one symbol would also influence its neighbors. But with the knowledge of the blood flow $V_R(t)$, all symbol boundaries can be derived from one parameter, i.e. the **transmission time** of the first symbol. Note that this is fundamentally different from the received time of the first symbol in a conventional wireless system, which also indicates another parameter—the TX-RX distance.

Returning to the above 1-D channel model with single-pulse CIR, where the TX-RX distance is δx and the flow rate is $v(t)$. Once the transmission time of the packet is known, the transmission time of each symbol can be derived by adding multiple symbol intervals, so the received time can be inferred by Equation 3 accordingly. Besides, the TX-RX distance δx can be achieved by detecting the received time of the first symbol and integrating the flow rate since its transmission. However, in a real molecular network in the blood, the CIR is never a single tap but with a certain delay spread, so the above TX-RX “distance” is implicitly included in the CIR.

FlowLink’s packet detection is composed of two stages:

- 1) **Coarse detection (time-axis)**. This is identical to the detection method in conventional wireless systems. Specifically, FlowLink maintains two back-to-back sliding windows of time samples, computes the power ratio of the signals in the two windows and seeks the time sample with the peak ratio. As discussed above, the symbol boundaries are warped due to the varying flow, so this

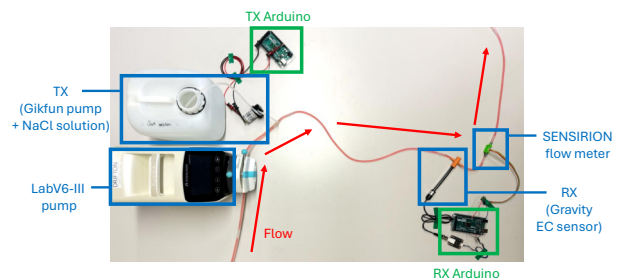


Fig. 6: FlowLink testbed. It simulates the blood vessel in the silicone tube architecture, with the LabV6-III pump providing a heartbeat-like periodic flow.

method does not provide an accurate signal received time, not to mention the transmitted time of the first symbol. But it does serve as a good starting point to proceed to the next finer detection step.

- 2) **Finer detection (flow-axis)**. Considering the influence of laminar flow, a non-negligible proportion of particles in a pulse would arrive at the receiver earlier than average since they are far away from the wall of vessels. This indicates that the molecular CIR generally has a non-negligible rising stage in power. So, the CIR delay spread should span both after and before the coarse detection, and the transmitted time of the first symbol is even earlier (Figure 5). Understanding this, FlowLink searches the transmission time in the samples earlier than the coarse detection, by estimating the flow-axis CIR and finding the one that best fits the original signal. Specifically, for the packet preamble \vec{p} and a tentative transmission time t , FlowLink first maps the time-axis preamble \vec{p}_t to the flow-axis version as was described in Section IV-A.

$$\vec{p}_t \mapsto \vec{p}_V \quad (6)$$

It is then used to construct the Toeplitz matrix $P = T(\vec{p}_V)$. The one that results in the minimum distance from the flow-axis signal \vec{y}_V to the column space of P will be the result of the finer detection.

$$\min_t \left\| \vec{y}_V - P(P^T P)^{-1} P^T \vec{y}_V \right\| \quad (7)$$

V. TESTBED

We build a testbed to simulate the blood vessel environment (Figure 6), with the following major components:

- **Channel**: Silicone tubes are used to simulate the blood vessels. It is also a common material in medical research and physician training due to its similarity to biological tissues. These tubes are cheap and highly flexible to be bent and connected to form any expected topology.
- **Medium**: Water is used in the testbed as the propagation medium, which is shown to share similar properties with human blood [44]. We do not filter the water, so the ions in the water can serve as a source of noise in the channel, similar to the particles that are involved with human body activities but will influence the receiver measurement.
- **Flow**: Blood flow is the highlighted feature in the blood network, so we use the Shenzhen LabV6-III peristaltic

pump to provide a periodic flow. The pump can take in commands from an RS485 interface and set the motor at a given rotating speed (Rounds Per Minute, RPM) to provide a specific flow. However, the command rate is limited by the RS485 protocol, which means that we cannot perfectly mimic a real blood flow. Instead, the actual flow in the experiments is a two-step function, with a high RPM phase for systole and a low one for diastole.

- **Information-bearing particle:** Sodium chloride ($NaCl$) serves as the information-bearing particle in this testbed due to two major concerns: first, it is easy to buy $NaCl$; and second, $NaCl$ is friendly to the environment, which demands no dedicated process before disposal.
- **Transmitter (TX):** $NaCl$ is stored as the solution of high concentration, which will be pressed into the main channel through a Gikfun pump. The Gikfun pump functions as the transmitter, which is powered on (through a transistor switch circuit) for a very short amount of time to send a bit “1”, and stays silent for a bit “0”. Its influence over the total amount of flow is negligible.
- **Receiver (RX):** The concentration of $NaCl$ is measured by the Gravity Analog Electrical Conductivity (EC) reader, which is at the downstream of the transmitter. It is connected to the tube with a specifically designed 3D printed cap, so the water can run through between the metal plates of the EC reader without leakage. Due to the spreading in the molecular channel, the high-concentration pulse from the transmitter has been diluted by the time it arrives at the receiver. Thus, the EC is approximately linear to the concentration of $NaCl$.
- **Flow meter:** Due to the architecture of the peristaltic pump, it cannot offer a strictly constant flow when the motor rotates within one round. Thus, we cannot use the commanded RPM as the flow speed. Instead, SENSIRION SEK-SLF3S-4000B is mounted after the receiver to provide ground truth flow measurement.
- **Control:** The transmitter and the receiver are controlled by two separate Arduino Mega 2560 rev3 with SD modules, while the LabV6-III pump is controlled through MATLAB. All three are synchronized over the serial communication on one laptop.

We have conducted extensive experiments with various parameters, including the inner diameter of the tube (mimicking common human small arteries), the packet symbol interval, the average rate and the HIGH-to-LOW duration ratio of the flow, the TX-RX distance and the channel topology, which will be presented immediately. Over 40 packets under each condition are collected, while each trace lasts for around two minutes. Packets of shorter symbol intervals have more bits.

VI. RESULTS

This chapter illustrates the performance of FlowLink with extensive experiments. Reviewing the key ideas of FlowLink, the most fundamental one is the re-sampling operation that transforms the signal from time scale into flow scale. Thus, we modify FlowLink’s decoder by removing the resampling

process and use it as the baseline, which is named decoder on “time-axis”. Correspondingly, FlowLink is named decoder on “flow-axis”.

This paper adopts two metrics to evaluate the performance of FlowLink:

- **Bit Error Ratio (BER)**—the number of bit errors divided by the total number of transferred bits. This is the common metric used to evaluate a communication system. The bar plot presents the BER when the original signal (time-axis) or the preprocessed signal (flow-axis) is taken as input by a state-of-the-art decoder [41], which reveals the BER of 10-th, 50-th (mean) and 90-th percentile. These results focus on the comparison between the two bars instead of the trending across different parameters, while the latter demands a larger dataset and deeper analysis.
- **Fitting error improvement.** Fitting error is defined as the Mean Squared Error (MSE) between the received signal and the reconstructed signal, while the latter is computed through convolution between ground truth transmitted bits and a CIR estimated from the packet. Large fitting error indicates bad performance, and the improvement is defined as the subtraction of the flow-axis error from the time-axis error. These results have nothing to do with the applied decoder afterwards, and reveals the general advantage of using flow-axis over time-axis.

Besides, two different cases are considered:

- Normal, where the receiver performs packet detection, channel estimation and decoding to finally receive the transferred bits. This is used to evaluate the overall performance of FlowLink.
- GTPD, Ground-Truth Packet-detection, where the receiver is assumed to know the exact transmission time of a packet, but needs to perform the rest steps.

A. Main results

We first present FlowLink’s overall performance in the setup simulating carotid artery. The channel is a single 10 cm tube of 4 mm ID, and the flow cycle is 12 mL/s (100 cm/s) for 0.3 seconds followed by 3 mL/s (25 cm/s) for 0.5 seconds. Under such conditions, we have collected data with different packet symbol intervals, i.e. 0.5/0.6/0.7/0.8/1.0/1.4 seconds.

Figure 7a shows the overall decoder performance under the normal decoding procedure. When the symbol interval is 0.5/0.6/0.7/0.8 seconds, there is a clear advantage of decoding on flow-axis over on time-axis, not only in average BER, but also the 10-th and 90-th percentile. However, such gain is not viewed when the symbol interval grows longer (1.0/1.4 seconds). The reason is that the BER under long symbol interval is too small to validate the advantage of FlowLink, so a larger dataset is needed for further validation.

1) *Flow-axis advantage:* To directly show the advantage of using flow-axis over time-axis, Figure 7b compares the BER under time-axis and flow-axis when the transmission time is known (GTPD). As we mentioned in Section IV-A, the flow-axis can present a coherent CIR for the whole packet while the time-axis cannot. To validate this claim, we show the decoding

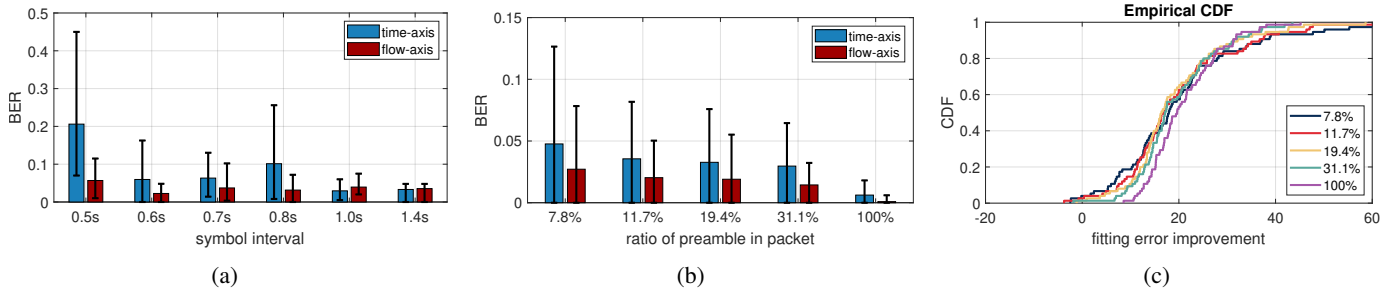


Fig. 7: Major results comparing the performance of FlowLink with flow-unaware decoder: (a) BER under different datarate, with normal decoding process); (b) BER under different proportion of preamble, with GTPD decoding process; (c) improvement in fitting error under different proportion of preamble, with GTPD decoding process

performance with regard to the proportion of the preamble to the whole packet. In fact, we process the same data (0.6 seconds symbol interval in Figure 7a, with 7.8% preamble), but intentionally treat part of the data symbols as preamble and decode the rest. The 100% data is a bit different—it decodes the original data symbols.

At first glance, we can observe that the BER goes down on both time-axis and flow-axis when the proportion of the preamble increases, which is a direct consequence of the increasing data samples for channel estimation. However, in the meanwhile, using time-axis can never achieve the same performance as flow-axis, because it only finds the best fitting CIR for the preamble, which cannot be generalized to the whole packet. Using the same data, Figure 7c also validates the claim through the perspective of fitting error. As the proportion of preamble increases, the fitting error improvement is less deviated from the median (around 20), which means the flow-axis advantage is maintained.

B. Micro Benchmarks

In the rest of this section, we will provide a few micro benchmarks showing the advantage of FlowLink under a few typical parameters, including the average flow rate, the background flow period, the TX-RX distance and the channel topology.

1) *Average flow rate:* Next, we will show FlowLink's performance with regard to the average flow rate. In the following experiments, the channel is a single 10 cm tube of 4 mm ID, and the symbol interval is 0.6 seconds. The basic flow cycle is 12 mL/s (100 cm/s) for 0.3 seconds followed by 3 mL/s (25 cm/s) for 0.5 seconds. The flow rate is scaled by 0.5/0.75/1.0/1.25 \times respectively, but the duration of each rate is kept the same.

As shown in Figure 8a, there is a clear decreasing trend in BER when the average flow rate is increasing. Faster flow reduces the propagation delay from the transmitter to the receiver. It also reduces the spreading of molecular signal due to laminar flow, which indicates decreasing Inter-Symbol Interference (ISI) and is the explanation for the decreasing BER. However, at all flow rates, the advantage of the flow-axis is clear. From another perspective, Figure 8b shows that as the flow rate increases, the fitting error improvement is more clustered around a lower but still positive value. Finally, it can

be inferred from these two figures that the time-axis BER will be good enough at high flow rate such that flow-axis process is no longer required.

2) *Flow period:* Since each individual has a different cardiac cycle, we take a close look on FlowLink's performance over blood flows of different period. In the following experiments, the channel is a single 10 cm tube of 4 mm ID, and the symbol interval is 0.8 seconds. The fast flow in the cycle is 12 mL/s (100 cm/s) for 0.3 seconds, but the slow flow is 3 mL/s (25 cm/s) for 0.4/0.5/0.6/0.7 seconds, so the total period is 0.7/0.8/0.9/1.0 seconds.

In Figure 9b, we can see that for all flow periods, at least 15% of the data shows improvement in the fitting error when adopting FlowLink. Correspondingly, Figure 9a shows the improvement in BER for all conditions. One thing to notice is that the growing flow period indicates more proportion of LOW flow in the cycle. This leads to the slower average flow speed and longer propagation delay. Intuitively, the overall BER is meant to increase because of the increasing ISI, like the trend of 0.7/0.8/1.0 seconds. However, 0.9 seconds yields an unusual trend, where the BER is much lower than its neighbors.

3) *TX-RX distance:* The TX-RX distance is another parameter that has an interesting relation with the flow. In the following experiments, the channel is a single tube of 4 mm ID, and the symbol interval is 0.6 seconds. The basic flow cycle is 12 mL/s (100 cm/s) for 0.3 seconds followed by 3 mL/s (25 cm/s) for 0.5 seconds. The distance between the transmitter and the receiver is varied among 10/15/20/25/30 cm.

In Figure 10b, we can see that for all TX-RX distances, at least 20% of the data shows improvement in the fitting error when adopting FlowLink. Correspondingly, In Figure 10a shows the improvement in BER for all conditions. However, there is an unusual trend in BER as a function of growing TX-RX distance. Intuitively, the direct consequence of the increasing TX-RX distance is the longer propagation delay, which will lead to more ISI and higher BER. But except for the 10 cm condition, other conditions reveal an opposite trend, i.e. the BER of 30 cm is lower than the BER of 15 cm. This is an interesting joint result of ISI and varying flow-ISI can partially compensate for the error in the sampling time. For a simple case when a single pulse function passes a channel

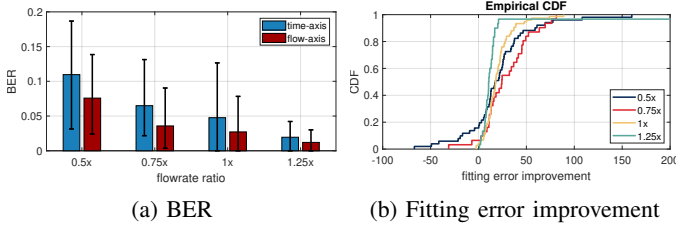


Fig. 8: The performance of FlowLink under different average flow rate, with GTPD decoding process.

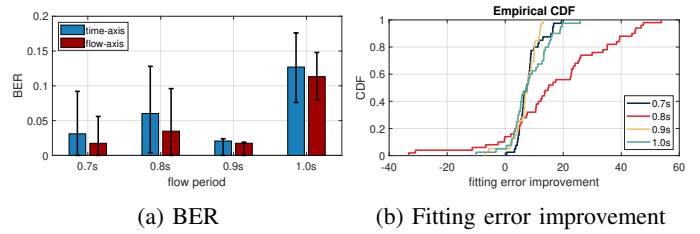


Fig. 9: The performance of FlowLink under different total flow period, with GTPD decoding process.

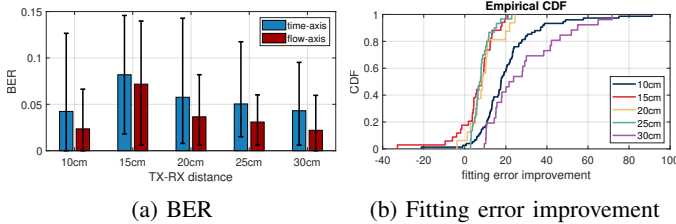


Fig. 10: The performance of FlowLink under different TX-RX distance, with GTPD decoding process.

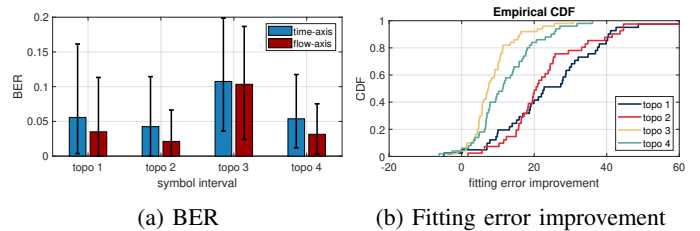


Fig. 11: The performance of FlowLink under four variants of the molecular channel, with GTPD decoding process.

without ISI (i.e. the received signal is also a pulse function), a minor error in the sampling time will return a zero value. On the contrary, a channel with ISI can tolerate such error under a certain threshold.

4) *Various channel topology*: As claimed in Section IV-A, FlowLink not only works for a simple channel of a single tube with a constant diameter, but can be generalized to more complicated topology. The following experiments test FlowLink's performance in four different vessel topologies, which are presented in Figure 12. They represent the basic channel variation in blood vessels, including narrowing (topo 1), widening (topo 2), forking (topo 3) and merging (topo 4). The tubes are connected with I-shape or Y-shape connectors. The dimension of the tubes and the distance between the transmitter/receiver and the connector are marked in the figure.

From Figure 11a, we can see that FlowLink shows clear improvement in decoding under topo 1/2/4. However, topo 3 is an exception, where the BER for both FlowLink and baseline are much worse than the other three topologies. By analyzing all four topologies, we can see that under topo 1/2/4, all particles released by the transmitter will pass the receiver detection range, but under topo 3, only a proportion of the information-bearing particles will go to the receiver fork. It is possible that this proportion is not a constant under the experimental periodic flow, which experiences sudden velocity change and might lead to unstable distribution around the forking. And that is why the time-axis decoder also encounters a bad performance. However, the advantage of FlowLink can still be validated through the fitting error improvement in Figure 11b. Further investigation is required on detailed flow measuring on both forks and better blood flow simulation.

VII. RELATED WORK

Blood network testbeds. There has been a lot of effort in simulating the blood network channel. [35], [40] used silicone

tubes to simulate the vessels and evaluate the performance of decoders, but were not strict with the flow speed. [34] used a 2-mm diameter silicone tube to simulate the vascular system with volume rates between 50 mL/min and 90 mL/min. [37] used a 3-mm diameter tube which is close to the average diameter of coronary artery with volume rates between 50 mL/min and 350 mL/min. [38] used a narrower 1.52-mm diameter tube and lower volume rates between 2 mL/min and 20 mL/min, but tested the propagation of the bio-compatible SPION particles. However, the above work only provided some results under constant flow rate and ignored the influence of flow variation due to heart beat.

Fast-varying channel in conventional communication systems. This paper, to our knowledge, is the first to address the fast-varying channel in molecular communication. But there have been various work for conventional wireless channels. Fast-varying channel was first officially considered in radio astronomy [45], [46], but has nowadays become a common phenomenon in most popular communication systems due to the rapidly growing mobility in different user scenarios. Besides, underwater acoustic communication views much higher relative Doppler shifts, since the sound speed in water is only around 1500 m/s [42]. [47] proposed a two-step approach to mitigate the Doppler influence in zero-padded OFDM for underwater acoustic communication, which includes a step of non-uniform resampling based on frequency-dependent Doppler drifts. [48] further demonstrated the effectiveness of Doppler-based resampling for underwater acoustic OFDM transmission without guard interval, but at a much lower-than-normal symbol rate. Despite the numerous solutions for conventional communication systems, none of them can be directly applied to MC, because the delay spread can be much longer than the channel coherence time in the blood network.

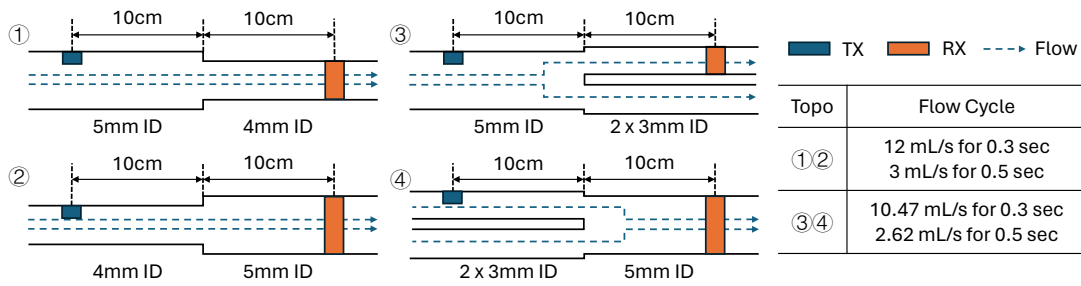


Fig. 12: Four variants of the molecular channel: narrowing (topo 1), widening (topo 2), forking (topo 3) and merging (topo 4). And the simulated flow under each condition.

VIII. DISCUSSIONS AND FUTURE WORK

A. Flow Sampling

Compared to conventional decoders, FlowLink employs a re-sampling operation in the first phase in order to recover linear assumptions in the molecular signal, such that conventional decoders can be applied. However, re-sampling is known to have outstanding drawbacks. On the one hand, from the communication perspective, re-sampling could lead to loss of information and aliasing because the molecular channel response is not band-limited. On the other hand, from the hardware point, resampling consumes extra computation and memory resources, which are both limited for bio-nano devices in the current theory. But, since we are still in a stage when hundreds of molecular communication theories sprout, can we dream bigger and dive into the possibilities of designing flow sampling architectures to replace the conventional time sampling? The advantage is obvious that the sampled signals can be directly applied to a linear decoder. Nevertheless, it also comes with new challenges. For example, the sampling flow interval should not be a unanimous number, which could lead to information loss due to the flow difference in a complex molecular channel topology. More studies are demanded before it could be concluded whether flow sampling is the right direction.

B. Complication of Blood Flow

The real blood vessel is a much more complicated system than what is studied in this paper, so a few assumptions do not always hold. First, laminar flow is not always true, and the contradictory is turbulence—unpredictable flow. Turbulence can lead to a similar influence as diffusion, but with a much larger coefficient. Whether a system is turbulent is usually described by the Reynolds number whose value in this testbed is around 300. Usually, a system with Reynolds number $Re < 2000$ is assumed mostly laminar. However, it is reported that there exists turbulence in physiological blood flow [49]. It is not only a driving factor for numerous diseases such as atherosclerosis, stenosis and aneurysm (large Reynolds number), but also is observed under common cases (low Reynolds number). This is a challenge to FlowLink, because diffusion is strongly related to time and its influence is twisted on flow-axis. It is the same for the possible chemical transformation of particles during propagation in a practical system. Second,

the possibility of reverse blood flow is ignored, which is another possible symptom of blood disease. FlowLink adopts the one-to-one mapping when there is no reverse flow, which is not the optimum choice for patients. How to use the flow-axis appropriately without losing any information is also a good topic. Third, the diameter of blood vessels is not time-invariant. For example, the muscle pumps with more blood flow during workouts. This would influence the topology of the blood network, especially forking and merging. It is worthwhile to study the influence of such variation, whether it can be circumvented and how to address the issue before the actual deployment of the blood network.

C. Flow estimation

Using flow meter for real-time speed tracking complicates the architecture of a practical molecular device, because it is an extra sensor from original functionality. However, flow speed estimation is possible with pure communication module by using two receivers—one in the upstream and one in the downstream. Each sample of the downstream signal is a delayed version of one in the upstream signal. By finding the matched samples and the time difference between them, a linear equation system on flow speed can be constructed and solved—which falls in the reign of Dynamic Time Warping (DTW) [50]. Besides, the distance between the two receivers need not be known, because FlowLink only cares about the relative flow variation. Moreover, the periodicity of the blood flow can also be employed to improve the estimation, together with either conventional methods or the uprising deep learning solutions (such as LSTM) that are proficient in time series processing.

IX. CONCLUSION

This paper is the first to identify the destructive influence of the blood flow on state-of-the-art decoders—the heart pumping behavior results in the drastically varying blood flow rate in each heartbeat cycle. This causes complicated symbol boundary drift at the receiver end, especially when the symbol rate is in the same order of the heartbeat rate. FlowLink is proposed to address this issue, where sampling based on the propagation flow, instead of a fixed time interval, compensates for the varying channel per symbol, which greatly improves the decoder performance.

REFERENCES

- [1] O. B. Akan, H. Ramezani *et al.*, "Fundamentals of molecular information and communication science," *Proceedings of the IEEE*, vol. 105, no. 2, pp. 306–318, 2016.
- [2] Y. Chahibi, M. Pierobon *et al.*, "A molecular communication system model for particulate drug delivery systems," *IEEE Trans. Biomed. Eng.*, vol. 60, no. 12, pp. 3468–3483, 2013.
- [3] Y. Chahibi, I. F. Akyildiz *et al.*, "Molecular communication modeling of antibody-mediated drug delivery systems," *IEEE Trans. Biomed. Eng.*, vol. 62, no. 7, pp. 1683–1695, 2015.
- [4] Y. Chahibi, M. Pierobon *et al.*, "Pharmacokinetic modeling and biodistribution estimation through the molecular communication paradigm," *IEEE Trans. Biomed. Eng.*, vol. 62, no. 10, pp. 2410–2420, 2015.
- [5] M. Kuscü, E. Dinc *et al.*, "Transmitter and receiver architectures for molecular communications: A survey on physical design with modulation, coding, and detection techniques," *Proceedings of the IEEE*, vol. 107, no. 7, pp. 1302–1341, 2019.
- [6] S. Salehi, N. S. Moayedian *et al.*, "Lifetime improvement of a multiple transmitter local drug delivery system based on diffusive molecular communication," *IEEE Trans. Nanobiosci.*, vol. 17, no. 3, pp. 352–360, 2018.
- [7] I. F. Akyildiz, M. Pierobon *et al.*, "The internet of bio-nano things," *IEEE Communications Magazine*, vol. 53, no. 3, pp. 32–40, 2015.
- [8] M. Kuscü, E. Dinc *et al.*, "Transmitter and receiver architectures for molecular communications: A survey on physical design with modulation, coding, and detection techniques," *Proceedings of the IEEE*, vol. 107, no. 7, pp. 1302–1341, 2019.
- [9] M. Kuscü and B. D. Unluturk, "Internet of bio-nano things: A review of applications, enabling technologies and key challenges," *arXiv preprint arXiv:2112.09249*, 2021.
- [10] M. Mimee, P. Nadeau *et al.*, "An ingestible bacterial-electronic system to monitor gastrointestinal health," *Science*, vol. 360, no. 6391, pp. 915–918, 2018.
- [11] P. Nadeau, M. Mimee *et al.*, "21.1 nanowatt circuit interface to whole-cell bacterial sensors," in *2017 IEEE ISSCC*. IEEE, 2017, pp. 352–353.
- [12] Y. Rajavi, M. Taghivand *et al.*, "An rf-powered fdd radio for neural microimplants," *IEEE J. Solid-State Circuits*, vol. 52, no. 5, pp. 1221–1229, 2017.
- [13] O. Jonas, H. M. Landry *et al.*, "An implantable microdevice to perform high-throughput in vivo drug sensitivity testing in tumors," *Science translational medicine*, vol. 7, no. 284, pp. 284ra57–284ra57, 2015.
- [14] E. Samiei, M. Tabrizian *et al.*, "A review of digital microfluidics as portable platforms for lab-on-a-chip applications," *Lab on a Chip*, vol. 16, no. 13, pp. 2376–2396, 2016.
- [15] A. Van Reenen, A. M. de Jong *et al.*, "Integrated lab-on-chip biosensing systems based on magnetic particle actuation—a comprehensive review," *Lab on a Chip*, vol. 14, no. 12, pp. 1966–1986, 2014.
- [16] T. Danino, O. Mondragón-Palomino *et al.*, "A synchronized quorum of genetic clocks," *Nature*, vol. 463, no. 7279, pp. 326–330, 2010.
- [17] D. M. Shcherbakova, A. A. Shemetov *et al.*, "Natural photoreceptors as a source of fluorescent proteins, biosensors, and optogenetic tools," *Annual review of biochemistry*, vol. 84, pp. 519–550, 2015.
- [18] B. Krishnaswamy, "Algorithms for molecular communication networks," Ph.D. dissertation, Georgia Institute of Technology, 2018.
- [19] J. E. Dahlman, K. J. Kauffman *et al.*, "Barcoded nanoparticles for high throughput in vivo discovery of targeted therapeutics," *Proceedings of the National Academy of Sciences*, vol. 114, no. 8, pp. 2060–2065, 2017.
- [20] H. Shi, K. Nie *et al.*, "Recent progress of microfluidic reactors for biomedical applications," *Chemical Engineering Journal*, vol. 361, pp. 635–650, 2019.
- [21] C. Steiger, A. Abramson *et al.*, "Ingestible electronics for diagnostics and therapy," *Nature Reviews Materials*, vol. 4, no. 2, pp. 83–98, 2019.
- [22] Medtronic, "Remote monitoring for implanted heart devices." [Online]. Available: <https://www.medtronic.com/us-en/patients/treatments-therapies/remote-monitoring.html>
- [23] J. S. McLean, "A re-examination of the fundamental limits on the radiation of electrically small antennas," *IEEE Trans. Antennas Propag.*, vol. 44, no. 5, p. 672, 1996.
- [24] D. F. Sievenpiper, D. C. Dawson *et al.*, "Experimental validation of performance limits and design guidelines for small antennas," *IEEE Trans. Antennas Propag.*, vol. 60, no. 1, pp. 8–19, 2011.
- [25] T. Yamada, T. Uezono *et al.*, "Rf attenuation characteristics for in vivo wireless healthcare chip," *Japanese journal of applied physics*, vol. 44, no. 7R, p. 5275, 2005.
- [26] T. S. Moon, C. Lou *et al.*, "Genetic programs constructed from layered logic gates in single cells," *Nature*, vol. 491, no. 7423, pp. 249–253, 2012.
- [27] B. D. Unluturk, A. O. Bicen *et al.*, "Genetically engineered bacteria-based biotransceivers for molecular communication," *IEEE Trans. Commun.*, vol. 63, no. 4, pp. 1271–1281, 2015.
- [28] R. Daniel, J. R. Rubens *et al.*, "Synthetic analog computation in living cells," *Nature*, vol. 497, no. 7451, pp. 619–623, 2013.
- [29] A. Tamsir, J. J. Tabor *et al.*, "Robust multicellular computing using genetically encoded nor gates and chemical 'wires,'" *Nature*, vol. 469, no. 7329, pp. 212–215, 2011.
- [30] P. Siuti, J. Yazbek *et al.*, "Synthetic circuits integrating logic and memory in living cells," *Nature biotechnology*, vol. 31, no. 5, pp. 448–452, 2013.
- [31] M. Fakruddin, Z. Hossain *et al.*, "Prospects and applications of nanobiotechnology: a medical perspective," *Journal of nanobiotechnology*, vol. 10, no. 1, pp. 1–8, 2012.
- [32] G. Rampioni, L. Leoni *et al.*, "Molecular communications in the context of 'synthetic cells' research," *IEEE Trans. Nanobiosci.*, vol. 18, no. 1, pp. 43–50, 2018.
- [33] S. Slomovic, K. Pardee *et al.*, "Synthetic biology devices for in vitro and in vivo diagnostics," *Proceedings of the National Academy of Sciences*, vol. 112, no. 47, pp. 14429–14435, 2015.
- [34] W. Pan, X. Chen *et al.*, "A molecular communication platform based on body area nanonetwork," *Nanomaterials*, vol. 12, no. 4, p. 722, 2022.
- [35] J. Wang, D. Hu *et al.*, "Understanding and embracing the complexities of the molecular communication channel in liquids," in *Proceedings of the 26th Annual International Conference on Mobile Computing and Networking*, 2020, pp. 1–15.
- [36] L. Wang and A. W. Eckford, "Nonnegative code division multiple access techniques in molecular communication," in *15th CWIT*, 2017, pp. 1–5.
- [37] M. Bayat, M. Mostafavi *et al.*, "Towards practical implementation of molecular communication: A cost-effective experimental platform based on the human circulatory system," *IET Communications*, 2024.
- [38] M. Bartunik, J. Teller *et al.*, "Channel parameter studies of a molecular communication testbed with biocompatible information carriers: Methods and data," *IEEE Transactions on Molecular, Biological and Multi-Scale Communications*, 2023.
- [39] F. Wang, P. Jin *et al.*, "Flexible doppler ultrasound device for the monitoring of blood flow velocity," *Science advances*, vol. 7, no. 44, p. eabi9283, 2021.
- [40] N. Farsad, D. Pan *et al.*, "A novel experimental platform for in-vessel multi-chemical molecular communications," in *GLOBECOM 2017*. IEEE, 2017, pp. 1–6.
- [41] J. Wang, S. Ögüt *et al.*, "Towards practical and scalable molecular networks," in *Proceedings of the ACM SIGCOMM 2023 Conference*, 2023, pp. 62–76.
- [42] F. Hlawatsch and G. Matz, *Wireless communications over rapidly time-varying channels*. Academic press, 2011.
- [43] G. Matz and F. Hlawatsch, "Time-varying communication channels: Fundamentals, recent developments, and open problems," in *2006 14th European Signal Processing Conference*. IEEE, 2006, pp. 1–5.
- [44] M. U. Mahfuz, D. Makrakis *et al.*, "On the characteristics of concentration-encoded multi-level amplitude modulated unicast molecular communication," in *2011 24th Canadian conference on electrical and computer engineering (CCECE)*. IEEE, 2011, pp. 000 312–000 316.
- [45] J. D. Kraus, M. Tiuri *et al.*, *Radio astronomy*. McGraw-Hill New York, 1966, vol. 66.
- [46] A. R. Thompson, J. M. Moran *et al.*, *Interferometry and synthesis in radio astronomy*. Springer Nature, 2017.
- [47] B. Li, S. Zhou *et al.*, *Non-uniform Doppler compensation for zero-padded OFDM over fast-varying underwater acoustic channels*. IEEE, 2007.
- [48] Y. V. Zakharov and A. K. Morozov, "Ofdm transmission without guard interval in fast-varying underwater acoustic channels," *IEEE J. Ocean. Eng.*, vol. 40, no. 1, pp. 144–158, 2014.
- [49] K. M. Saqr, S. Tupin *et al.*, "Physiologic blood flow is turbulent," *Scientific reports*, vol. 10, no. 1, p. 15492, 2020.
- [50] D. Dürrenmatt, D. Del Giudice *et al.*, "Dynamic time warping improves sewer flow monitoring," *Water research*, vol. 47, no. 11, pp. 3803–3816, 2013.